Supporting Information

Room-temperature Synthesis and CO_2-Gas Sensitivity of Bismuth Oxide Nanosensors

Pritamkumar V. Shinde[a], Nanasaheb M. Shinde[b], Shoyebmohamad F. Shaikh[d], Je Moon Yun[b], Lee Jung Woo[c], Abdullah M. Al-Enizi[d]*, Rajaram S. Mane[ae]*, and Kwang Ho Kim[ab]*

[a]Global Frontier R&D Center for Hybrid Interface Materials, [b]National Core Research Center, and [c]School of Materials Science and Engineering Pusan National University, 30, Jangjeon-dong, Geumjung-gu, Busan 609-735, Republic of Korea.

[d] College of Science, Department of Chemistry, King Saud University, Riyadh 11451, Saudi Arabia

[e]School of Physical Sciences, Swami Ramanand Teerth Marathwada University, Nanded, Nanded, Maharashtra, India.

Corresponding Author. mane3796@pusan.ac.kr (Rajaram Mane, Prof.),

amenizi@ksu.edu.sa (A. M. Al-Enizi, Prof.), and kwhokim@pusan.ac.kr (K. H. Kim, Prof.)

S1

Characterizations

The physical elucidation and morphological analysis of Bi_3O_2 nanostructures were performed by using X-ray diffraction patterns (Bruker D8 discover XRD diffractometer using Cu Kα radiation (λ = 1.5406 Å) at 40 kV and 40 mA), field-emission scanning electron microscopy (FE-SEM, Hitachi, S-4800, 15 kV) images equipped with energy-dispersive X-ray spectroscopy (EDX), and high-resolution transmission electron microscopy (HRTEM, JEOL 2100F) with the selected area electron diffraction (SAED) (Technai F20) techniques, respectively. The X-ray photoelectron spectroscopy (XPS, VG Scientifics ESCALAB250) measurement was performed to analyze the chemical bonding information of Bi-O. The Brunauer–Emmett–Teller (BET) and Barrett–Joyner–Halenda (BJH) measurement plots obtained using the Micrometrics ASAP2010 analyzer were used to obtain the surface area and pore-size distributions of the powder scratched from the respective Bi_2O_3-film-sensor surfaces.

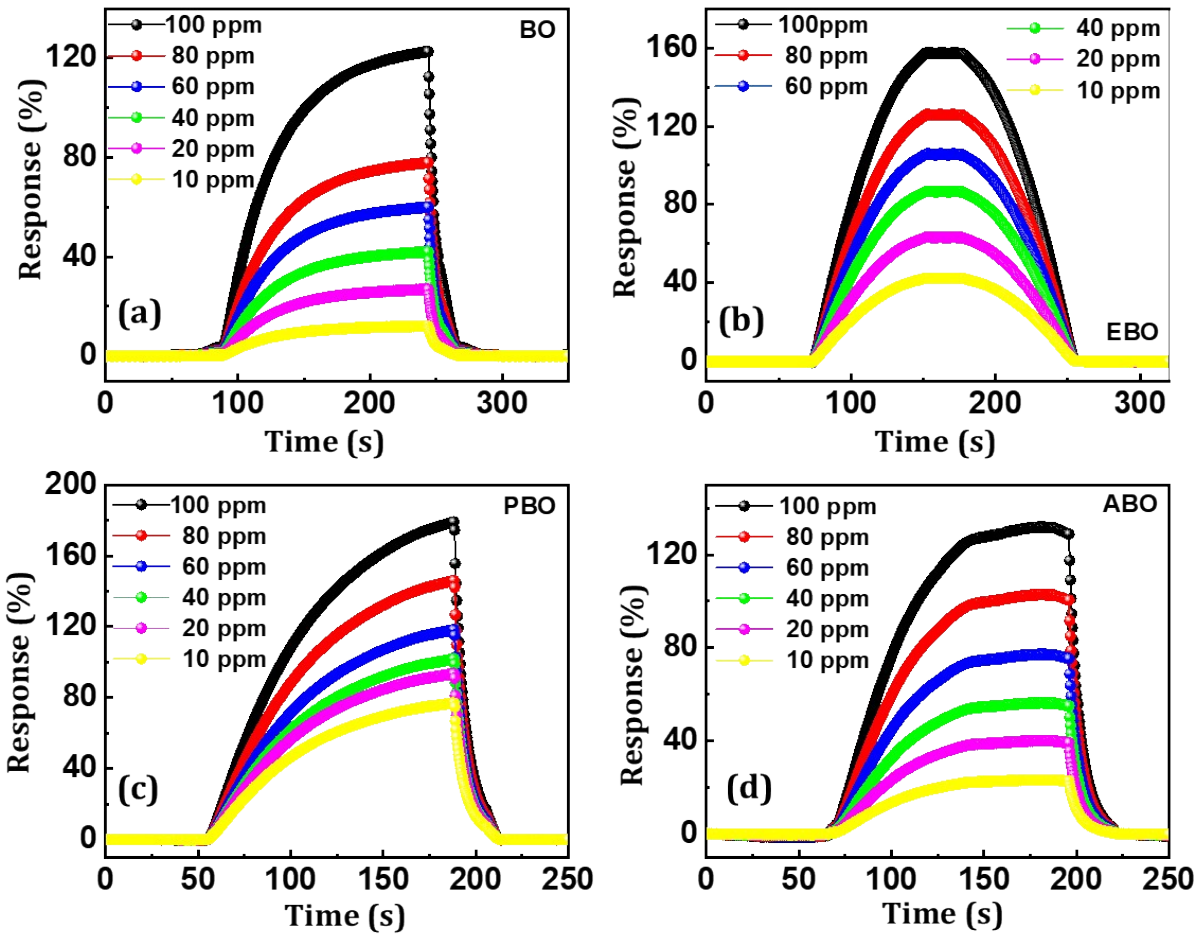

Figure S1. The response vs. time (at different 10-100 ppm) of the (a) BO, (b) PBO, (c) EBO, and (d) ABO film sensors

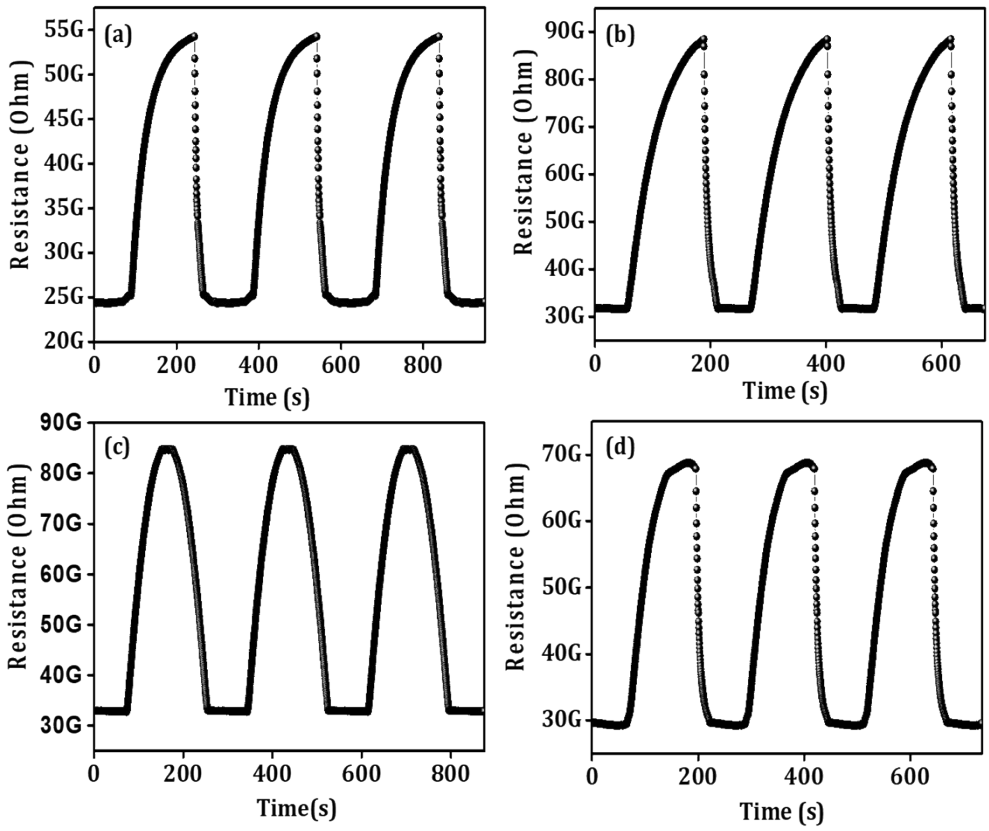

Figure S2. The repeatability of transient vs. time (at 100 ppm) of the BO, PBO, EBO and ABO film sensors

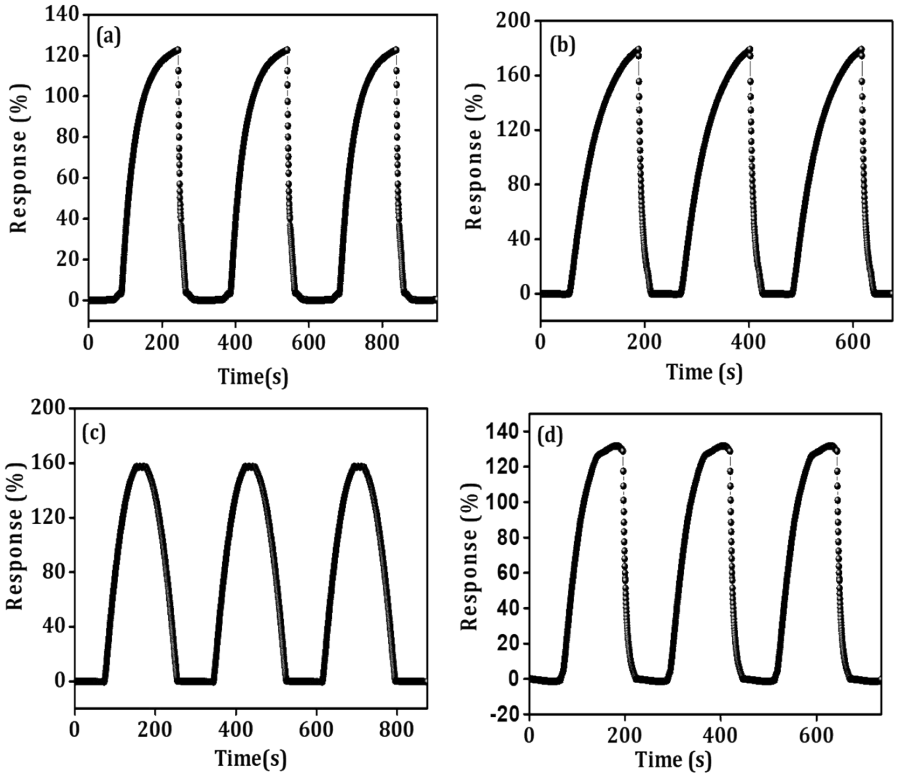

Figure S3. The repeatability of response vs. time (at 100 ppm) of the (a) BO, (b) PBO, (c) EBO, and (d) ABO film sensors

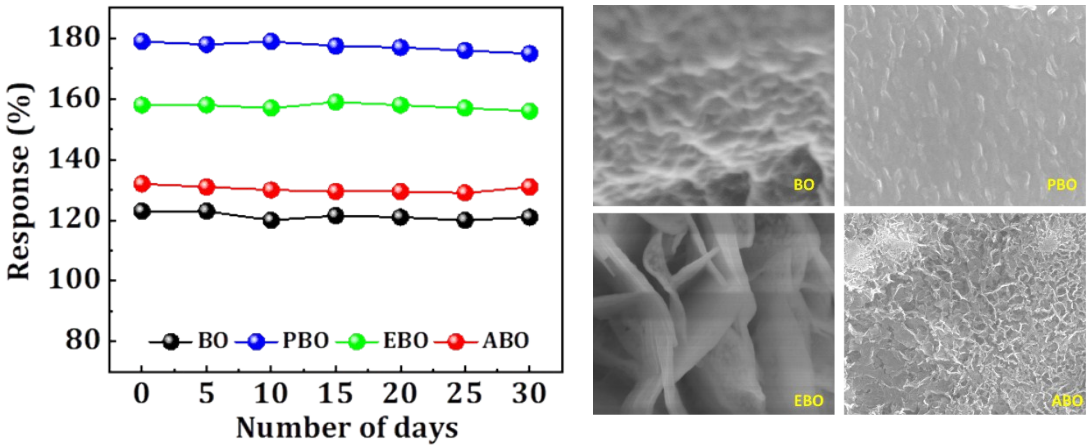

(a) **(b)**

Figure. S4 (a)Stability measurements of the BO, PBO, EBO, and ABO film sensors (b) after sensing experiments morphological stability of the BO, PBO, EBO, and ABO film sensors

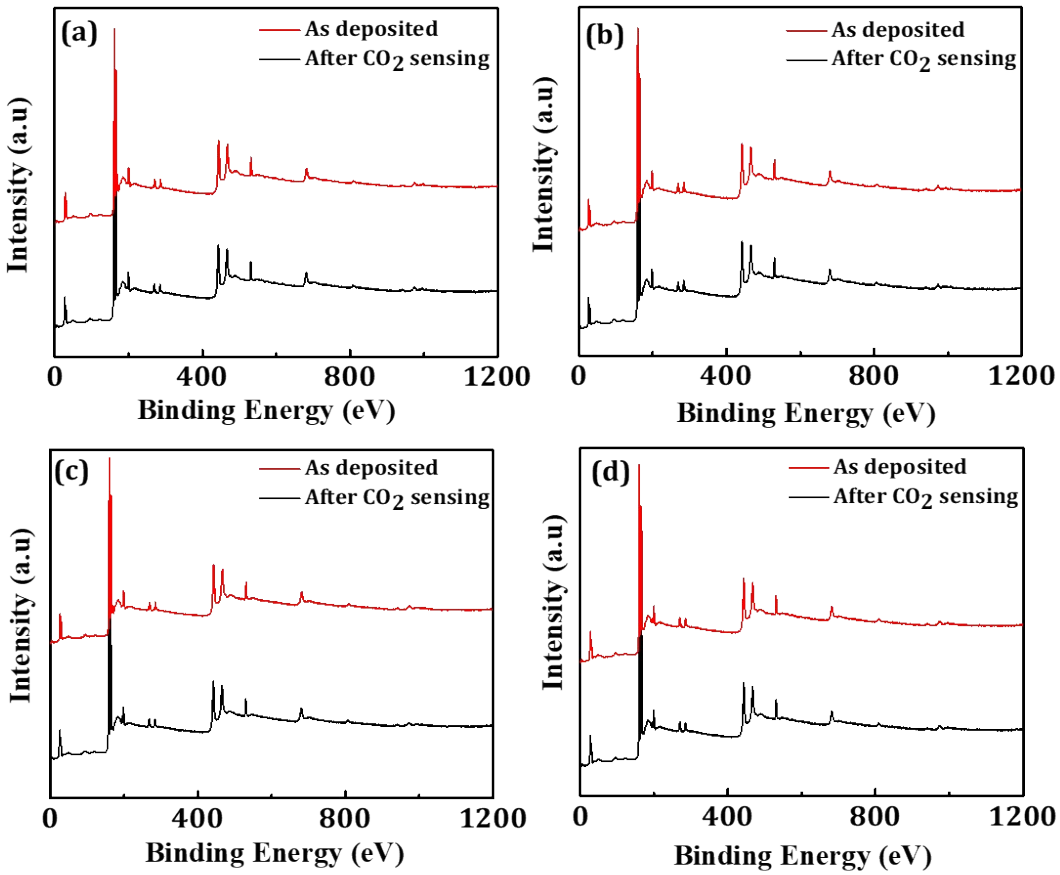

Figure. S5. Survey XPS before and after gas sensing of (a) BO, (b) PBO, (c) EBO, and (d) ABO film sensors

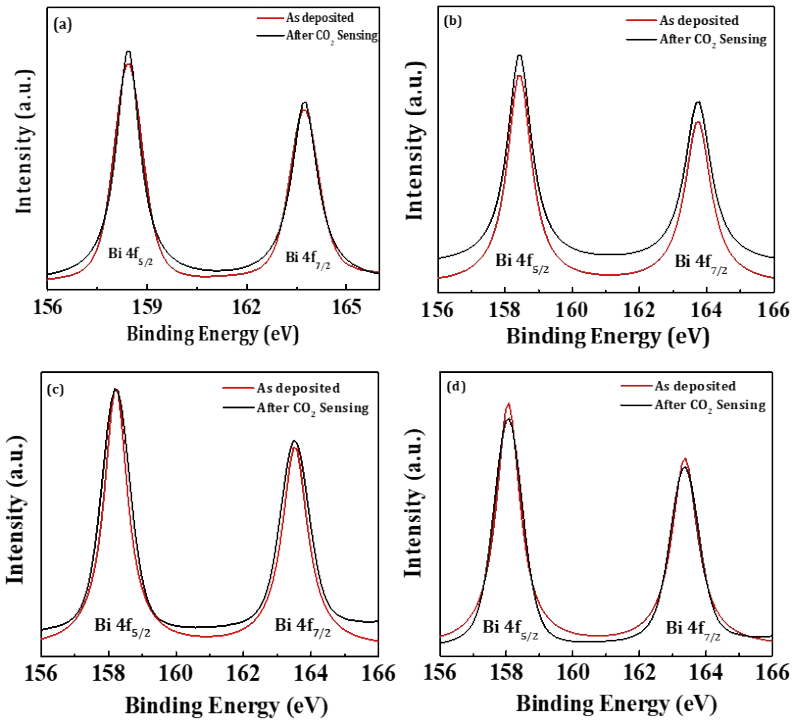

Figure. S6. Enlarged XPS spectra of Bi4f before and after gas sensing of (a) BO, (b) PBO, (c) EBO, and (d) ABO film sensors

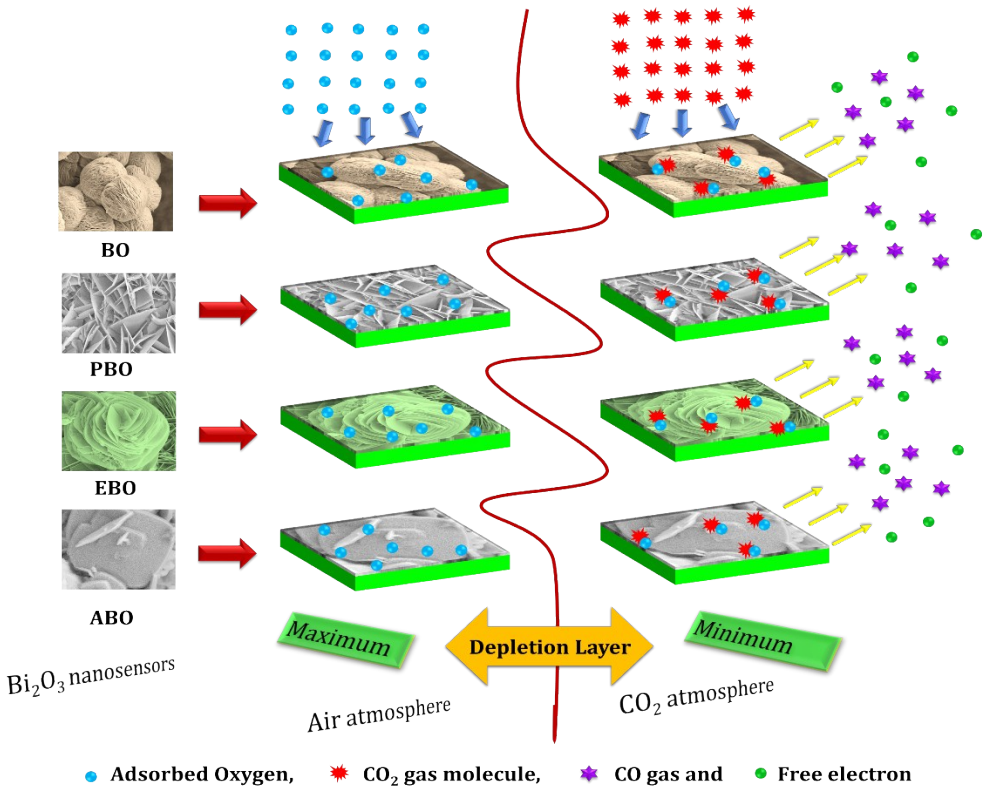

Figure. S7. The gas sensing mechanism of the BO, PBO, EBO and ABO nanosensors in air and in the presence of CO_2 gas.

Table S1 Compared present work with the previously reported data on CO_2 gas sensing.

Sr. No.	Material	Structure	Synthesis method	C (ppm)	S (%)	t_{res}/t_{rec} (s)	Temp	Ref.
1	graphene	Nanosheet	Stamping method	100	26	8/10	60	S1
2	rGO-F20	Smooth nanosheet	Hydrogen plasma method	1500	15	~240/240	23	S2
3	La_2O_3	Micro rod	CBD	350	48	50/73	250	S3
4	La_2O_3	Honeycomb	Spray pyrolysis	500	68	180/125	300	S4
5	La_2O_3	Web-like nanoparticles	Ultrasonic spray pyrolysis	300	75	80/141	225	S5
6	La_2O_3	Nanorod	Microwave-Assisted	400	25	80/50	450	S6
7	Pd: La_2O_3	Disk on Nanorod	Microwave-Assisted	400	64	80/50	250	S6
8	Bi_2O_3	Nanoporous	Anodization	100	77	-	27	S7
9	β-Bi_2O_3	Nanoplates	CBD	1000	100	40/50	150	S8

10	BO	Woolen globes	CBD	100	123	77/82	27	
11	PBO	Nano sheets	CBD	100	179	132/82	27	
12	ABO	Flower-rose	CBD	100	158	151/28	27	Present Work
13	EBO	Spongy square plates	CBD	100	132	89/32	27	

C = concentration; t_{res}/t_{rec} = response time/recovery time; and S % = Gas Response in %

References

S1 H. J. Yoon, J. H. Yang, Z. Zhou, S. S. Yang, and M. M.C. Cheng, Carbon dioxide gas sensor using a graphene sheet. Sens. and Actuators B, 157 (2011) 310–313.

S2 S. M. Hafiz, R. Ritikos, T. J. Whitcher, N. M. Razib, D. C. S. Bien, N. Chanlek, H. Nakajima, T. Saisopa, P. Songsiriritthigul, N. M. Huang, S. A. Rahman, A practical carbon dioxide gas sensor using room-temperature hydrogen plasma reduced graphene oxide. Sens. Actuators B, 193 (2014) 692–700.

S3 A. Yadav, A. C. Lokhande, J. H. Kim and C. D. Lokhande, Highly sensitive CO_2 sensor based on microrods-like La_2O_3 thin film electrode. RSC Adv., 6 (2016) 106074.

S4 A. Yadav, A. C. Lokhande, R. B. Pujari, J. H. Kim, C. D. Lokhande, The synthesis of multifunctional porous honey comb-like La_2O_3 thin film for supercapacitor and gas sensor applications. J Colloid Intrf Sci., 484 (2016) 51–59.

S5 A. A. Yadav, V. C. Lokhande, R. N. Bulakhe and C.D. Lokhande, Amperometric CO_2 gas sensor based on interconnected web-like nanoparticles of La_2O_3 synthesized by ultrasonic spray pyrolysis. Microchim. Acta, 184 (2017) 3713-3720.

S6 A. A. Yadav, A. C. Lokhande, J. H. Kim, C. D. Lokhande, Enhanced sensitivity and selectivity of CO_2 gas sensor based on modified La_2O_3 nanorods. J. Alloy and Compd, 723 (2017) 880–886.

S7 M. Ahila, J. Dhanalakshmi, J. C. Selvakumari and D. P. Padiyan, Heat treatment effect on crystal structure and design of highly sensitive room temperature CO_2 gas sensors using anodic Bi_2O_3 nanoporous formed in a citric acid electrolyte.Mater. Res. Express, 3 (2016) 105025.

S8 S. S. Bhande, R. S. Mane, A. V. Ghule and S. H. Han, A bismuth oxide nanoplate-based carbon dioxide gas sensor.Scr. Mater. 65 (2011) 1081–1084.